Journal of Materials Chemistry A

PAPER

View Article Online
View Journal | View Issue

Check for updates

Cite this: J. Mater. Chem. A, 2017, 5, 19773

Synthesis, properties, and photovoltaic characteristics of p-type donor copolymers having fluorine-substituted benzodioxocyclohexene-annelated thiophene†

Yutaka Ie,*[ab] Koki Morikawa,[a] Makoto Karakawa,‡[a] Naresh B. Kotadiya,[b] Gert-Jan A. H. Wetzelaer,*[b] Paul W. M. Blom*[b] and Yoshio Aso*[a]

The incorporation of an acceptor unit into π-conjugated systems is an effective approach to tune both the highest occupied molecular orbital (HOMO) and the lowest unoccupied molecular orbital (LUMO) energy levels of organic semiconducting materials. We report on the design of a series of fluorine-substituted benzodioxocyclohexene-annelated thiophene acceptor units and the synthesis of donor–acceptor (D–A) type copolymers based on these acceptor units and dithienosilole as a donor unit. Physical measurements of the copolymers indicate that the D–A characteristics are increased by increasing the number of introduced fluorine atoms and the HOMO and LUMO energy levels of the copolymers are fine-tuned depending on the acceptor units. Organic photovoltaics based on blend films of these D–A copolymers and [6,6]-phenyl-C_{71}-butyric acid methyl ester show photovoltaic responses with a power conversion efficiency of up to 7.30%. Investigation of the device physics shows that the performance is mainly limited by the hole transport, which provides insight in the direction of material design toward the improvement of OPV performance. These results demonstrate the potential of fluorine-substituted benzodioxocyclohexene-annelated thiophene as an acceptor unit in organic semiconducting materials.

Received 5th July 2017
Accepted 21st August 2017

DOI: 10.1039/c7ta05822e

rsc.li/materials-a

Open Access Article. Published on 22 August 2017. Downloaded on 7/28/2025 9:54:58 AM.
This article is licensed under a Creative Commons Attribution 3.0 Unported Licence.

Introduction

π-Conjugated polymers and structurally well-defined small molecules have been extensively developed for application in semiconducting materials in organic thin-film electronics such as organic field-effect transistors (OFETs) and organic photovoltaics (OPVs).[1–6] Both hole-transporting (p-type) and electron-transporting (n-type) organic semiconductors are required for the fabrication of these devices. It has been well-established that electrons or holes can be selectively injected by tuning the relative energies between the Frontier orbital of organic semiconductors and the Fermi level of metal electrodes. Thus, tuning of both the highest occupied molecular orbital (HOMO) and the lowest unoccupied molecular orbital (LUMO) energy level is important.[2] The straightforward approach to tune the HOMO and LUMO energy levels is the incorporation of electron-accepting π-conjugated units into π-conjugated systems.[1–5] However, effective electron-accepting π-conjugated units for this purpose are still limited due to the difficulty of molecular design, which fulfills both the electron-accepting character and effective conjugation in the resulting π-conjugated systems.[7–16]

We previously reported that dihexyl-substituted naphtho[2,3-*c*]thiophene-4,9-dione (**C_6**) is effective as an electron-accepting unit in π-conjugated materials applicable to n-channel OFETs.[17] Furthermore, the **C_6** unit can also function effectively as an acceptor unit of donor–acceptor (D–A) type copolymers for bulk-heterojunction OPVs. As a representative example, the D–A copolymer (**DTS-C_6**), being composed of dithieno[3,2-*b*:2′,3′-*d*]silole (**DTS**)[18–20] and **C_6** as donor and acceptor units, respectively, showed good photovoltaic characteristics.[21–23] With **DTS-C_6** as a p-type donor material in combination with [6,6]-phenyl-C_{71}-butyric acid methyl ester ($PC_{71}BM$) as an n-type acceptor, 7.85% power conversion efficiency (PCE) has been attained after precise optimization of the film-forming method.[22] This result motivated us to modify the chemical structure of **C_6** toward stronger electron-accepting nature,[24–27] which will lead to a decreased HOMO energy level of the copolymers. This is expected to result in an increased open-circuit voltage (V_{oc}) in OPVs because it has been suggested

[a]The Institute of Scientific and Industrial Research (ISIR), Osaka University, 8-1 Mihogaoka, Ibaraki, Osaka 567-0047, Japan. E-mail: yutakaie@sanken.osaka-u.ac.jp
[b]Max Planck Institute for Polymer Research, Ackermannweg 10, 55128 Mainz, Germany

† Electronic supplementary information (ESI) available: Detailed synthetic procedures and characterization data of new compounds and additional experimental results. See DOI: 10.1039/c7ta05822e

‡ Present address: Institute for Frontier Science Initiative, Kanazawa University, Kakuma-machi, Kanazawa, Ishikawa 920-1192, Japan.

Open Access Article. Published on 22 August 2017. Downloaded on 7/28/2025 9:54:58 AM.
This article is licensed under a Creative Commons Attribution 3.0 Unported Licence.

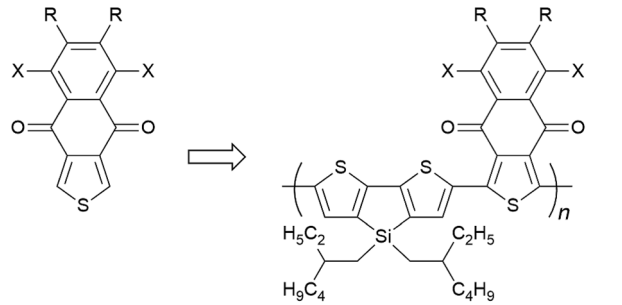

Fig. 1 Chemical structures of the acceptor units and copolymers used in this study.

that the V_{oc} is directly proportional to the energy-level difference between the HOMO of the p-type donor and the LUMO of the n-type acceptor.[28] Furthermore, the increased D–A character will reduce the band gap extending the light absorption to the long-wavelength region. To exemplify this hypothesis, we introduced strongly electron-withdrawing fluorine atoms into the benzene ring of $\mathbf{C_6}$ and designed $\mathbf{C_0(F_2)}$, $\mathbf{C_0(F_4)}$, and $\mathbf{C_6(F_2)}$ as new acceptor units (Fig. 1). We also designed $\mathbf{C_0}$ as a reference to these units.[29] In this contribution, these acceptor units were integrated into conjugated copolymers with **DTS** as a donor (**DTS-C$_0$**, **DTS-C$_0$(F$_2$)**, **DTS-C$_0$(F$_4$)**, and **DTS-C$_6$(F$_2$)**) to examine the influence of fluorine atoms on the polymer properties and OPV characteristics. Furthermore, the blend-film property investigation gave an insight into a way for the improvement of OPV performance based on copolymers containing the $\mathbf{C_0(F_2)}$ unit.

Results and discussion

Synthesis

The synthesis of target copolymers is shown in Scheme 1. 2-Bromo-1,4-difluorobenzene (**1**) was successively alkylated to obtain 1,4-difluoro-2,3-dihexylbenzene (**3d**). The dibromides of acceptor units **5a–5d** were obtained by Friedel–Crafts acylation between **3a–3d** and 2,5-dibromothiophene-3,4-dicarbonyl dichloride (**4**). Finally, copolymers **DTS-C$_0$**, **DTS-C$_0$(F$_2$)**, **DTS-C$_0$(F$_4$)**, and **DTS-C$_6$(F$_2$)** were synthesized *via* a microwave-assisted Stille coupling reaction between **5a–5d** and **DTS-Sn** in the presence of $Pd_2(dba)_3$ and P(*o*-tol)$_3$ in toluene at 180 °C for 40 min. These copolymers were isolated by consecutive Soxhlet extractions using methanol, acetone, and hexane to remove low-molecular weight components, followed by extraction using chloroform ($CHCl_3$). All the copolymers were soluble in common organic solvents such as $CHCl_3$, chlorobenzene, and *o*-dichlorobenzene (*o*-DCB). The number-average molecular weights (M_n) of the copolymers were determined by gel permeation chromatography (GPC) using $CHCl_3$ as an eluent with a polystyrene standard. As summarized in Table 1, all the copolymers showed high molecular weights of more than 30 kg mol^{-1} and narrow molecular-weight dispersities (D_M) of 1.2–1.6 (Table 1). The detailed synthesis and characterization including GPC charts and NMR spectra are described in the ESI†. Thermogravimetric analysis (TGA) showed that all the copolymers have a good thermal stability, with 5%-weight-loss temperatures (T_d) of over 360 °C (Fig. S1 in the ESI,† Table 1).

Photophysical properties

The electronic absorption spectra of **DTS-C$_0$**, **DTS-C$_0$(F$_2$)**, **DTS-C$_0$(F$_4$)**, and **DTS-C$_6$(F$_2$)** as well as a reference copolymer **DTS-C$_6$** in both dilute $CHCl_3$ solutions and films are shown in Fig. 2.[22] The photophysical data including the absorption maximum

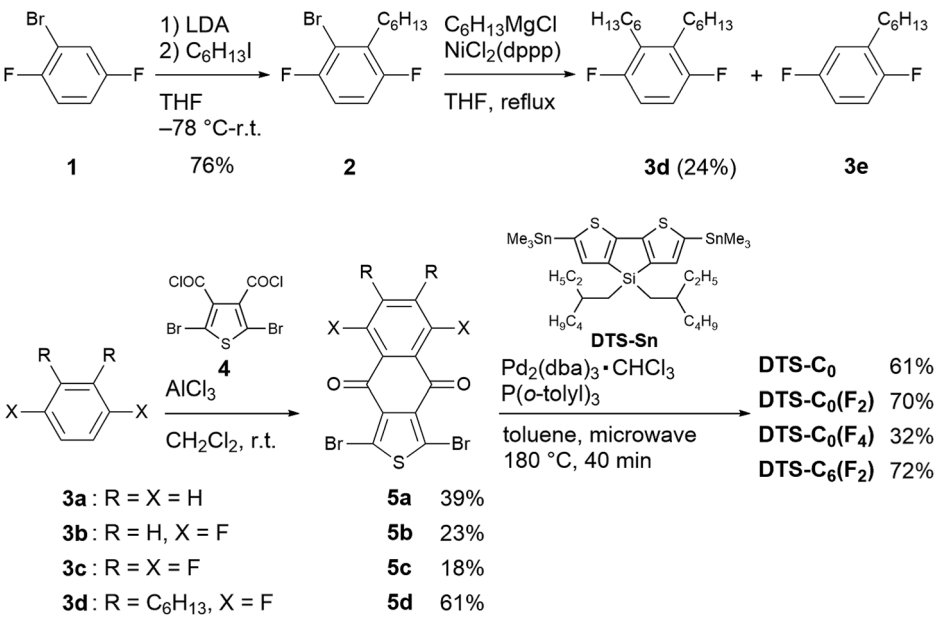

Scheme 1 Synthesis of target copolymers.

 This journal is © The Royal Society of Chemistry 2017

Open Access Article. Published on 22 August 2017. Downloaded on 7/28/2025 9:54:58 AM.
This article is licensed under a Creative Commons Attribution 3.0 Unported Licence.

Table 1 Properties of compounds

Compounds	M_n/kg mol^{-1}	D_M	T_d/°C	λ_{max}[a]/nm	λ_{onset}[b]/nm	ΔE_{opt}[c]/eV	E_{HOMO}[d]/eV	E_{LUMO}[e]/eV	$\mu_h^{copolymer}$/m^2 V^{-1} s^{-1}
DTS-C$_0$	35.3	1.49	365	607	755	1.64	−5.37	−3.73	5.1×10^{-9}
DTS-C$_0$(F$_2$)	31.6	1.62	395	611	779	1.59	−5.44	−3.85	1.1×10^{-8}
DTS-C$_0$(F$_4$)	36.6	1.48	409	631	816	1.51	−5.59	−4.07	3.5×10^{-9}
DTS-C$_6$(F$_2$)	36.8	1.29	364	609	751	1.65	−5.37	−3.72	3.9×10^{-9}
DTS-C$_6$[f]	42.8	1.70	412	598	765	1.62	−5.25	−3.63	1.2×10^{-8}

[a] In $CHCl_3$. [b] In films. [c] $\Delta E_{opt} = 1240/\lambda_{onset}$. [d] Determined by PESA measurements. [e] Determined by E_{HOMO} and ΔE_{opt}. [f] Ref. 22.

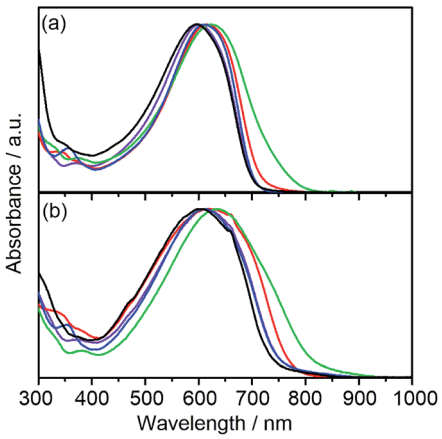

Fig. 2 UV-vis spectra of DTS-C$_0$ (purple), DTS-C$_0$(F$_2$) (red), DTS-C$_0$(F$_4$) (green), DTS-C$_6$(F$_2$) (blue), and the reference polymer DTS-C$_6$ (black) in (a) $CHCl_3$ solution and (b) thin films.

(λ_{max}) in solution, absorption onset (λ_{onset}) in films, and the HOMO–LUMO energy gap (ΔE_{opt}) estimated from λ_{onset} are summarized in Table 1. Compared with **DTS-C$_0$** and **DTS-C$_6$**, the λ_{max}s of the corresponding fluorinated copolymers **DTS-C$_0$(F$_2$)** and **DTS-C$_6$(F$_2$)** are red-shifted. Furthermore, by increasing the number of fluorine atoms (**DTS-C$_0$**, **DTS-C$_0$(F$_2$)**, and **DTS-C$_0$(F$_4$)**), a progressive clear red-shift of λ_{max} was observed, indicating that the fluorine atoms in the acceptor units have a certain influence on the absorption owing to the increased D–A character. The absorption spectra of the copolymer films were broadened and obviously red-shifted in comparison with those in the solutions, indicating the appearance of intermolecular interactions in the solid state, which is beneficial for charge-carrier transport. Particularly, λ_{onset} in the film of **DTS-C$_0$(F$_2$)** showed a significant red shift compared to the λ_{onset} in solution, indicating that **DTS-C$_0$(F$_2$)** might have better intermolecular interaction in the solid state. In addition, **DTS-C$_0$** and **DTS-C$_0$(F$_4$)** also showed a large red-shift from solution to the solid state. These results indicate that the removal of substituents from the benzene part of the acceptor unit reduces steric bulkiness and thus induces intermolecular electronic interactions. Consequently, HOMO–LUMO energy gaps (ΔE_{opt}s) can be controlled by modifying the acceptor unit with electron-withdrawing fluorine substituents, that is, ΔE_{opt} of the copolymers is reduced sequentially as the electron deficiency of the acceptor unit is increased.

Frontier-orbital energy levels

The HOMO energy levels (E_{HOMO}s) of all copolymers in the film state were estimated by photo-electron spectroscopy in air (PESA) as shown in Fig. 3. The E_{HOMO}s of the copolymers were decreased with increasing the number of electron-withdrawing fluorine substituents or removal of electron-donating hexyl chains in the acceptor unit (Table 1). The LUMO energy level (E_{LUMO}) was estimated by the addition of ΔE_g^{opt} to E_{HOMO} (Table 1). E_{LUMO} was more significantly decreased with the addition of fluorine atoms compared with E_{HOMO}, which means that fluorine substituents on the benzene part of the acceptor units more strongly affect the LUMO as compared to the HOMO of the copolymers. The resulting energy level diagram of all copolymers is shown in Fig. 4.

Carrier mobility

The hole mobility of donor polymers plays an important role in the OPV performance. In order to evaluate the hole mobility (μ_h)

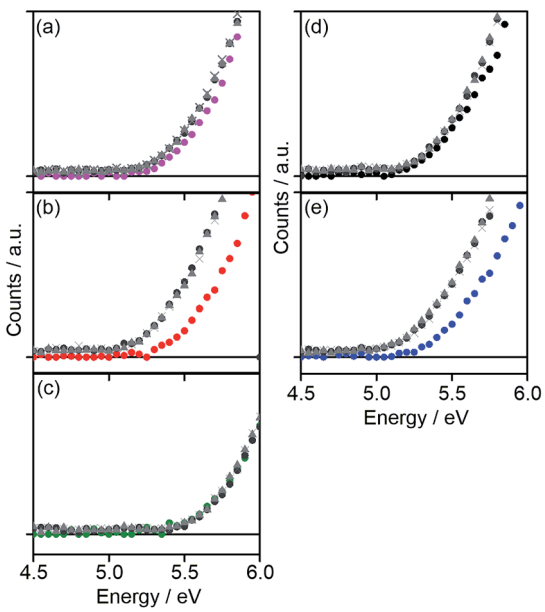

Fig. 3 PESA of (a) DTS-C$_0$ (pink circle), (b) DTS-C$_0$(F$_2$) (red circle), (c) DTS-C$_0$(F$_4$) (green circle), (d) DTS-C$_6$ (black circle), and (e) DTS-C$_6$(F$_2$) (blue circle) pristine films. PESA of the copolymer:$PC_{71}BM$ blend films in the weight ratio of 1 : 1 (brown circle), 1 : 2 (brown triangle), and 1 : 3 (brown cross) are also shown here.

Open Access Article. Published on 22 August 2017. Downloaded on 7/28/2025 9:54:58 AM.
This article is licensed under a Creative Commons Attribution 3.0 Unported Licence.

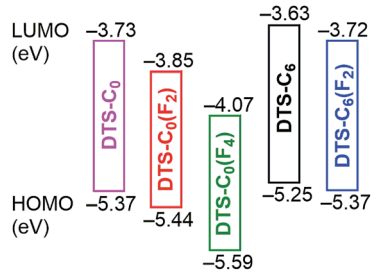

Fig. 4 Energy diagram of the copolymers.

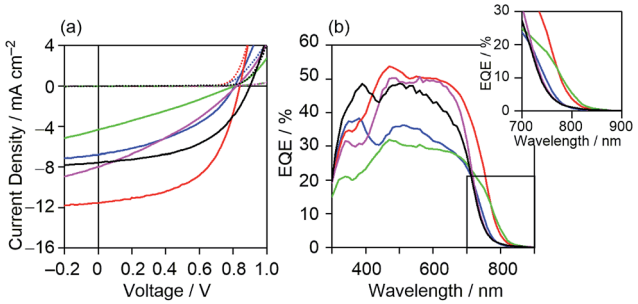

Fig. 5 (a) *J*–*V* characteristics under illumination (solid line) and in the dark (dashed line) and (b) EQE spectra of **DTS-C$_0$**:PC$_{71}$BM (pink), **DTS-C$_0$(F$_2$)**:PC$_{71}$BM (red), **DTS-C$_0$(F$_4$)**:PC$_{71}$BM (green), **DTS-C$_6$**:PC$_{71}$BM (black), and **DTS-C$_6$(F$_2$)**:PC$_{71}$BM (blue) blend films.

of the pristine copolymer films, hole-only devices with a configuration of indium tin oxide (ITO)/poly(3,4-ethylenedioxythiophene):poly(styrenesulfonate) (PEDOT:PSS)/copolymer/Au were fabricated, and μ_h was estimated using the space charge limited current (SCLC) model. Note that these films did not show any clear peaks in X-ray diffraction (XRD), indicating the formation of amorphous films. As summarized in Table 1, the copolymer **DTS-C$_0$(F$_2$)** exhibited one order of magnitude higher μ_h than those of other newly developed copolymers and similar to that of **DTS-C$_6$**, being expected to show high OPV performance among these copolymers.

Photovoltaic characteristics

To investigate the characteristics of newly synthesized copolymers as OPV donor materials, we fabricated a conventional device structure of glass/ITO/PEDOT:PSS/active layer/Ca/Al. The active layers consisted of a blend of the copolymer as a donor and PC$_{71}$BM as an acceptor. The fabrication conditions of the active layer were optimized to be the copolymer:PC$_{71}$BM blend composition of a 1 : 2 weight ratio, a concentration of 30 mg mL^{-1} in *o*-DCB with the use of 3% 1,8-diiodooctane (DIO) for spin-coating (Table S1, Fig. S2†), and without thermal annealing. All the measurements were performed under simulated AM 1.5G solar irradiation (100 mW cm^{-2}) in a nitrogen atmosphere. The best-performance current density–voltage (*J*–*V*) characteristic of each of the copolymers is shown in Fig. 5(a) and their key photovoltaic parameters are summarized in Table 2. All the data to ascertain the reproducibility of OPV performance are

Table 2 Photovoltaic characteristics of the copolymer:PC$_{71}$BM films

Blend films	J_{sc}/mA cm^{-2}	V_{oc}/V	FF/%	PCE[a]/%
DTS-C$_0$:PC$_{71}$BM	8.72	0.84	35	2.55 (2.34)
DTS-C$_0$(F$_2$):PC$_{71}$BM	11.58	0.84	54	5.28 (5.21)
DTS-C$_0$(F$_4$):PC$_{71}$BM	4.32	0.81	28	0.99 (0.96)
DTS-C$_6$(F$_2$):PC$_{71}$BM	6.79	0.80	42	2.26 (2.22)
DTS-C$_0$(F$_2$):PC$_{71}$BM[b]	16.71	0.86	51	7.30 (7.23)
DTS-C$_6$:PC$_{71}$BM[c]	10.59	0.90	55	5.21 (5.05)

[a] The average of 4 devices is provided in parentheses, see the ESI for details. [b] After optimization of the device structure and fabrication conditions. Active layers were fabricated using a 33 mg mL^{-1} solution in *o*-DCB with 3% DIO. [c] Ref. 22.

summarized in Fig. S3 and Tables S2–S6.† As shown in these data, all the copolymer-based devices showed typical photovoltaic responses. However, the device based on **DTS-C$_0$(F$_4$)**:PC$_{71}$BM showed the lowest short circuit current density (J_{sc}) among the investigated devices, leading to the lowest PCE of 0.99%. This low J_{sc} is caused by the lower LUMO energy level of **DTS-C$_0$(F$_4$)**, relative to that of PC$_{71}$BM, which prevents efficient charge separation from the photoexcited state of the copolymer. The removal of hexyl groups (**DTS-C$_0$**) or the introduction of fluorine atoms (**DTS-C$_6$(F$_2$)**) from or to the **C$_6$** unit did not contribute to the increase in J_{sc}. On the other hand, the **DTS-C$_0$(F$_2$)**:PC$_{71}$BM-based device showed an improved J_{sc} of 11.58 mA cm^{-2} compared to that of **DTS-C$_6$**:PC$_{71}$BM under the same fabrication conditions (10.59 mA cm^{-2}). Examination of the external quantum efficiency (EQE) spectra in Fig. 5(b) revealed the generation of a broad photocurrent in a longer wavelength region for **DTS-C$_0$(F$_2$)**:PC$_{71}$BM and **DTS-C$_0$**:PC$_{71}$BM with maximum EQEs of approximately 50%, whereas both **DTS-C$_0$(F$_4$)**:PC$_{71}$BM and **DTS-C$_6$(F$_2$)**:PC$_{71}$BM devices gave much lower EQE responses. Although the overall shapes of these EQE spectra well reflect the UV-vis absorption spectra of the corresponding blend films (Fig. S4†), photocurrent generation in the region exceeding 800 nm in the case of **DTS-C$_0$(F$_2$)**:PC$_{71}$BM is particularly significant, since this region exceeds the absorption onset of the pristine **DTS-C$_0$(F$_2$)** film (779 nm). As summarized in Table S7,† the difference in absorption onsets between the pristine and blend films is prominent for **DTS-C$_0$(F$_2$)** and **DTS-C$_6$(F$_2$)**, which may indicate the appearance of strong intermolecular interactions between copolymers and PC$_{71}$BM in the blend films. When focusing on the V_{oc}, no clear relationship against the E_{HOMO}s of copolymers was observed. We will discuss this point in a later section. Based on these OPV results, we further optimized the **DTS-C$_0$(F$_2$)**:PC$_{71}$BM-based device and found that the MeOH treatment of the active layer[30,31] and the use of a Ba thin cathode buffer layer instead of Ca led to 7.30% PCE with a J_{sc} of 16.71 mA cm^{-2}, V_{oc} of 0.86 V, and FF of 0.51. For the comparison with simulation, *J*–*V* characteristics are shown in Fig. 11.

Blend-film properties

In order to investigate the film morphology, atomic force microscopy (AFM) measurements of the blend films were

 This journal is © The Royal Society of Chemistry 2017

Open Access Article. Published on 22 August 2017. Downloaded on 7/28/2025 9:54:58 AM.
This article is licensed under a Creative Commons Attribution 3.0 Unported Licence.

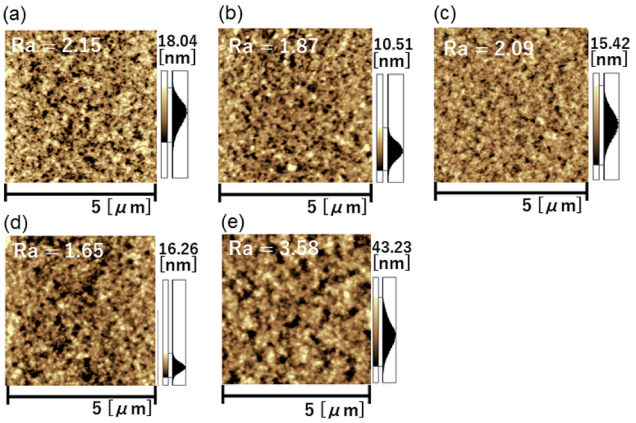

Fig. 6 AFM height images of (a) **DTS-C$_0$**:PC$_{71}$BM, (b) **DTS-C$_0$(F$_2$)**:PC$_{71}$BM, (c) **DTS-C$_0$(F$_4$)**:PC$_{71}$BM, (d) **DTS-C$_6$**:PC$_{71}$BM, and (e) **DTS-C$_6$(F$_2$)**:PC$_{71}$BM blend films.

carried out. As shown in Fig. 6, the **DTS-C$_6$(F$_2$)**:PC$_{71}$BM film showed relatively large grains, while the other blended films showed favorable smooth surfaces with the average roughness (R_a) between 1.65 and 2.09 nm. Since we have suggested that the surface free energies (SFEs) of the donor and the acceptor influence the properties of the donor/acceptor interface, we estimated SFEs of the copolymers and PC$_{71}$BM by the utilization of contact angle measurements.[32–34] As summarized in Table S8,† the SFEs as well as the contributions of the London dispersion (γ_d) and polar (γ_p) components of the copolymers were in a narrow range, suggesting that similar surface natures of the copolymer films rationalize the formation of similar blend-film interfaces and thus morphologies in combination with PC$_{71}$BM. In X-ray diffraction (XRD) measurements, no obvious diffraction peaks could be observed for all the blend films (Fig. S5†), indicating that these thin films have an amorphous nature. These results indicate that variation in the chemical structure of the acceptor unit in copolymers with DTS has little influence on the blend-film morphological properties.

The V_{oc} of OPVs is expected to be directly proportional to the difference between E_{HOMO} of the donor and E_{LUMO} of the acceptor. However, the V_{oc} of **DTS-C$_0$(F$_2$)**:PC$_{71}$BM-based OPVs was lower than that obtained from **DTS-C$_6$**:PC$_{71}$BM-based devices (0.84 V *vs.* 0.90 V), irrespective of the low-lying E_{HOMO} for **DTS-C$_0$(F$_2$)**. To investigate the origin of this unexpected phenomenon, we measured the PESA of blend films with different copolymer/PC$_{71}$BM ratios of 1 : 1, 1 : 2, and 1 : 3 (Fig. 3). As summarized in Fig. 7, the E_{HOMO}s of 1 : 1 blend films for **DTS-C$_0$(F$_2$)**:PC$_{71}$BM and **DTS-C$_6$(F$_2$)**:PC$_{71}$BM were increased compared to those of the corresponding copolymer pristine films (1 : 0), while the blend ratio has little influence on their E_{HOMO}s. On the other hand, the E_{HOMO}s of **DTS-C$_0$**, **DTS-C$_6$**, and **DTS-C$_0$(F$_4$)** did not show significant changes under these conditions. This result indicates that **DTS-C$_0$(F$_2$)** and **DTS-C$_6$(F$_2$)** might induce intermolecular interactions with PC$_{71}$BM, which were also suggested from the difference in their absorption onsets between pristine and blend films, and the resulting increase of E_{HOMO} in the mixed state caused the decrease of the V_{oc} in the OPVs. In addition, as shown in Fig. S6,† the dark *J*–*V* characteristics of **DTS-C$_0$(F$_2$)**:PC$_{71}$BM and **DTS-C$_6$(F$_2$)**:PC$_{71}$BM showed higher current density compared to those of other films. This phenomenon might be due to the influence of intermolecular charge-transfer interactions.

To get deeper insight into the device physics, we focused on the best-performance **DTS-C$_0$(F$_2$)**:PC$_{71}$BM devices. First, we measured the photocurrent (J_{ph}) of OPVs as a function of effective applied voltage (V_{eff}) under the light intensity of 10 and 100 mW cm^{-2}. The J_{ph} is given by the equation $J_{ph} = J_L - J_D$, where J_L and J_D are the current densities under illumination and dark conditions, respectively. The effective voltage V_{eff} is calculated as $V_{eff} = V_0 - V$, where V_0 is the voltage at $J_{ph} = 0$ and V is the applied bias. In this way, the effect of an electric field on the generated free carriers can be studied. As shown in Fig. 8, the photocurrent gradually increases with increasing effective voltage, which is characteristic of a recombination-limited photocurrent. It is observed that J_{ph} does not saturate even at high effective voltages. This is explained by a field-dependent dissociation rate of electron–hole pairs, or, in other words, field-dependent geminate recombination, giving rise to moderate fill factors.

The dominant geminate recombination process is confirmed by light-intensity-dependent measurements of the short-circuit current, as displayed in Fig. 9(a). The dependence of J_{sc} on P is described by the relationship $J_{sc} \propto P^{\alpha}$, where a deviation from

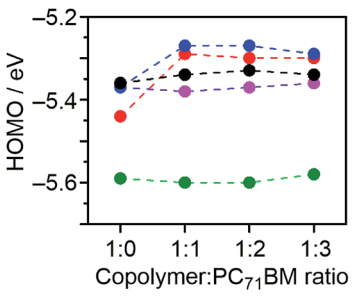

Fig. 7 Plots of the HOMO energy levels of films estimated from PESA against the blend ratio of copolymer:PC$_{71}$BM for **DTS-C$_0$**:PC$_{71}$BM (pink), **DTS-C$_0$(F$_2$)**:PC$_{71}$BM (red), **DTS-C$_0$(F$_4$)**:PC$_{71}$BM (green), and **DTS-C$_6$**:PC$_{71}$BM (black) and **DTS-C$_6$(F$_2$)**:PC$_{71}$BM (blue).

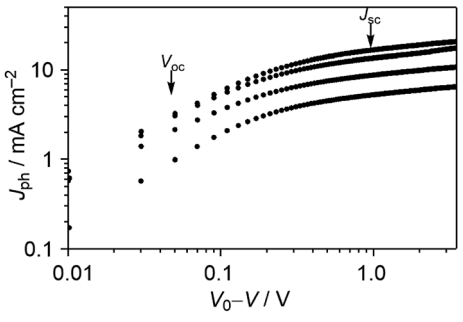

Fig. 8 J_{ph}–V_{eff} characteristics of **DTS-C$_0$(F$_2$)**:PC$_{71}$BM devices under illumination of a simulated solar spectrum. The arrows indicate the points of V_{oc} and J_{sc} conditions under 100 mW cm^{-2} irradiation conditions.

Open Access Article. Published on 22 August 2017. Downloaded on 7/28/2025 9:54:58 AM.
This article is licensed under a Creative Commons Attribution 3.0 Unported Licence.

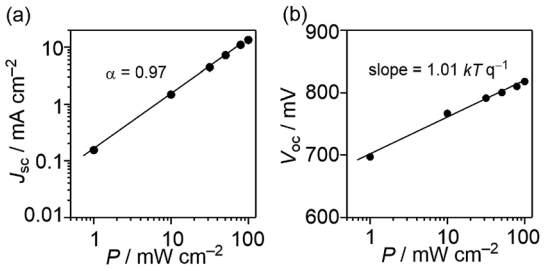

Fig. 9 Light-intensity (P) dependence of (a) J_{sc} and (b) V_{oc} for DTS-$C_0(F_2)$:$PC_{71}BM$ devices.

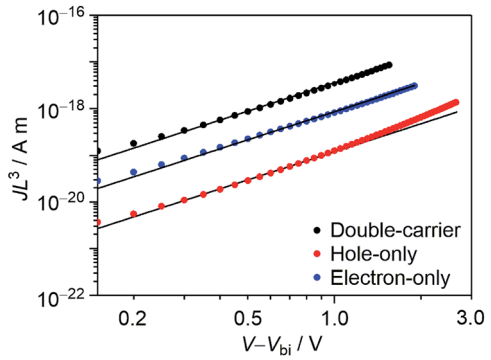

Fig. 10 Plots of JL^3 against $V - V_{bi}$ for DTS-$C_0(F_2)$:$PC_{71}BM$ at 295 K. Corresponding calculated results are shown in the straight line. Film thicknesses of double-carrier, holy-only, and electron-only devices are 85, 88, and 55 nm, respectively.

a linear relationship ($\alpha = 1$) is considered to be due to bimolecular-recombination losses.[35–37] In Fig. 9(a), we plotted the J_{sc} against light intensity, resulting in $\alpha = 0.97$. The small deviation from unity indicates that bimolecular recombination losses are minor under short-circuit conditions. Therefore, the increasing photocurrent beyond short-circuit conditions must be ascribed to a geminate-recombination process.

To investigate whether trap-assisted recombination plays a role, we also investigated the light-intensity dependence of V_{oc}. Since all photogenerated carriers recombine in the cell at V_{oc} ($J = 0$), the dependence of V_{oc} on the light intensity (P) gives information on the recombination process. In the case of bimolecular recombination, it has been reported that the slope of V_{oc} against the logarithm of P equals kTq^{-1}, where k is Boltzmann's constant, T is the temperature, and q is the elementary charge.[35,38] This slope increases when trap-assisted recombination is present.[39] The V_{oc} of the **DTS-$C_0(F_2)$**:$PC_{71}BM$-based device as a function of P between 1.0 mW cm^{-2} and 100 mW cm^{-2} is shown in Fig. 9(b). A slope of 1.01 kTq^{-1} was determined, indicating that trap-assisted recombination is effectively absent.

As can be observed from Fig. 8, the dissociation of electrons and holes is complicated in this system, which might be caused by poor charge transport. To reveal the charge-transport characteristics, we fabricated double-carrier, hole-only, and electron-only devices by using Au/PEDOT:PSS/**DTS-$C_0(F_2)$**:$PC_{71}BM$/Ba/Al, Au/PEDOT:PSS/**DTS-$C_0(F_2)$**:$PC_{71}BM$/MoO_3/Al, and Al/**DTS-$C_0(F_2)$**:$PC_{71}BM$/Ba/Al configurations, respectively. The observed J–V characteristics between 213 K and 295 K are shown in Fig. S7,† and the plots of JL^3 against $V - V_{bi}$, where L is the film thickness and V_{bi} is the built-in voltage are shown in Fig. 10. By using the SCLC equation, double-carrier (μ_{eff}), hole (μ_h), and electron (μ_n) mobilities of this blend film at 295 K were calculated to be 1.2×10^{-7}, 4.0×10^{-9}, and 3.0×10^{-8} m^2 V^{-1} s^{-1}, respectively. While the electron mobility is in the expected range for transport through $PC_{71}BM$, the hole mobility through the polymer phase appears to be relatively low.

Based on the mobility values and the equation:

$$\gamma_{pre} = \frac{16\pi}{9} \frac{\mu_p \mu_n}{\mu_{eff}^2 - (\mu_p + \mu_n)^2}$$

the Langevin prefactor (γ_{pre}) at 295 K is determined to be 5.1×10^{-2}.[40] The Langevin prefactor determines the deviation from a Langevin recombination rate. The found value indicates that the bimolecular-recombination rate is reduced by a factor of 20 with respect to Langevin recombination.

With the mobilities and bimolecular-recombination rate known, we simulated the J–V characteristics of **DTS-$C_0(F_2)$**:$PC_{71}BM$ devices under illumination with a drift-diffusion model (Fig. 11).[41] While the fill factor is well described, the voltage-dependent photocurrent at negative voltages is not reproduced. The reason for the poor description is the fact that the generation rate (G) of electrons and holes was considered field independent, whereas Fig. 8 suggests a field-dependent generation rate. To get an accurate fit to the experimental data, a field dependent generation rate has to be included according to the Onsager–Braun theory.[42] By using a charge-transfer state decay rate k_f of 1.0×10^6 s^{-1} and an initial separation distance of electron–hole pairs a of 1.9 nm, the experimental data are well described. The experimental values for the mobilities and Langevin prefactor were used. The simulation once more confirms that, next to bimolecular recombination, field-dependent electron–hole dissociation is responsible for the poor fill factors in the solar cell, giving rise to strong geminate recombination losses under operating conditions. We

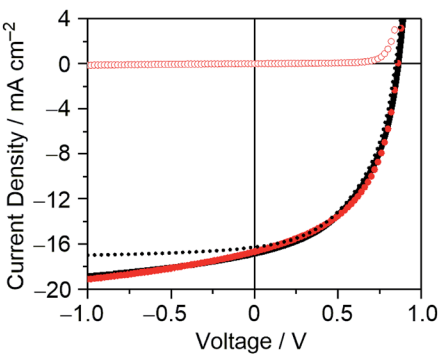

Fig. 11 J–V characteristics of the optimized DTS-$C_0(F_2)$:$PC_{71}BM$-based OPV device under illumination (filled red circle) and in the dark (red circle). Simulated J–V curves with a field-dependent and field-independent generation rate are shown in solid and dashed black lines, respectively.

This journal is © The Royal Society of Chemistry 2017

Open Access Article. Published on 22 August 2017. Downloaded on 7/28/2025 9:54:58 AM.
This article is licensed under a Creative Commons Attribution 3.0 Unported Licence.

postulate that the relatively poor hole transport inhibits efficient electron–hole pair separation.

As shown in Fig. S8,† there is a significant difference in temperature dependence between hole and electron mobilities. Activation energies of 0.22 eV and 0.36 eV were determined for electron and hole transport, respectively. In combination with the one order of magnitude lower hole mobility than electron mobility, this suggests more energetic disorder for hole transport. In view of the difficult separation of electrons and holes at the donor–acceptor interface, we concluded that the most critical point to determine the photovoltaic performance in a **DTS-C$_0$(F$_2$)**:PC$_{71}$BM system is the relative low hole mobility. In other words, the molecular design to increase the hole mobility using **DTS** and **C$_0$(F$_2$)** as donor and acceptor units may lead to an increase in the PCEs in terms of improving J_{sc} and FF.

Conclusions

In summary, we described here the synthesis and electronic properties of a series of new D–A type copolymers having fluorine-substituted naphtho[2,3-*c*]thiophene-4,9-diones as acceptor units. The fluorine substitution in naphtho[2,3-*c*]thiophene-4,9-dione chromophores contributes to a reduced band gap and low-lying HOMO energy level of the D–A copolymers, and we revealed that the photophysical properties as well as the energy levels are precisely controlled by the number of substituted fluorine atoms. All the copolymers exhibited photovoltaic characteristics in combination with PC$_{71}$BM, and high efficiencies of up to 7.30% were obtained for **DTS-C$_0$(F$_2$)**. The XRD and AFM measurements of the blend films indicated that all the films showed an amorphous character and similar morphologies. The detailed investigation of **DTS-C$_0$(F$_2$)**:PC$_{71}$BM device characteristics based on light-intensity dependent measurements and carrier mobility measurements as well as simulation of the *J*–*V* characteristics suggested that the increase of hole mobility becomes the key issue to improve the PCE. These results demonstrate the potential of fluorine-substituted naphtho[2,3-*c*]thiophene-4,9-dione units, and studies on the development of second-generation copolymers containing these units with improved hole mobility are underway in our laboratories.

Conflicts of interest

There are no conflicts to declare.

Acknowledgements

This work was supported by a Grant-in-Aid for Scientific Research (B) (16H04191) and Innovative Areas (JP25110004) from the Ministry of Education, Culture, Sports, Science and Technology, Japan. This work was partly supported by the Japan Society of Promotion Science (JSPS) Core-to-Core Program, A. Advanced Research Networks as well as JSPS Program for Advancing Strategic International Networks to Accelerate the Circulation of Talented Researchers. We are thankful to Prof. Y. Murata and Dr A. Wakamiya, Institute for Chemical Research (ICR) in Kyoto University, for PESA measurements and the Collaborative Research Program of the ICR in Kyoto University (grant 2016-37, 2017-38). Thanks are extended to the Comprehensive Analysis Center (CAC), ISIR, for assistance in obtaining elemental analyses and high-resolution mass spectroscopy.

Notes and references

1 Y.-J. Cheng, S.-H. Yang and C.-S. Hsu, *Chem. Rev.*, 2009, **109**, 5868–5923.
2 Y. Li, *Acc. Chem. Res.*, 2012, **45**, 723–733.
3 J.-S. Wu, S.-W. Cheng, Y.-J. Cheng and C.-S. Hsu, *Chem. Soc. Rev.*, 2015, **44**, 1113–1154.
4 J. Roncali, P. Leriche and P. Blanchard, *Adv. Mater.*, 2014, **26**, 3821–3838.
5 Y. Lin and X. Zhan, *Acc. Chem. Res.*, 2016, **49**, 175–183.
6 S. Holliday, J. E. Donaghey and I. McCulloch, *Chem. Mater.*, 2014, **26**, 647–663.
7 J. H. Hou, M. Park, S. Zhang, Y. Yao, L. Chen, J. Li and Y. Yang, *Macromolecules*, 2008, **41**, 6012–6018.
8 Y. Zhang, S. K. Hau, H.-L. Yip, Y. Sun, O. Acton and A. K.-Y. Jen, *Chem. Mater.*, 2010, **22**, 2696–2698.
9 Y. Zou, A. Najari, P. Berrouard, S. Beaupré, R. B. Aïch, Y. Tao and M. Leclerc, *J. Am. Chem. Soc.*, 2010, **132**, 5330–5331.
10 Y. Liang, Y. Wu, D. Feng, S.-T. Tsai, H.-J. Son, G. Li and L. Yu, *J. Am. Chem. Soc.*, 2009, **131**, 56–57.
11 H.-Y. Chen, J. H. Hou, S. Zhang, Y. Liang, G. Yang, Y. Yang, L. Yu, Y. Wu and G. Li, *Nat. Photonics*, 2009, **3**, 649–653.
12 M. Wang, X. Hu, P. Liu, W. Li, X. Gong, F. Huang and Y. Cao, *J. Am. Chem. Soc.*, 2011, **133**, 9638–9641.
13 I. Osaka, M. Shimawaki, H. Mori, I. Doi, E. Miyazaki, T. Koganezawa and K. Takimiya, *J. Am. Chem. Soc.*, 2012, **134**, 3498–3507.
14 C. Cui, X. Fan, M. Zhang, J. Zhang, J. Min and Y. Li, *Chem. Commun.*, 2011, **47**, 11345–11347.
15 D. Qian, L. Ye, M. Zhang, Y. Liang, L. Li, Y. Huang, X. Guo, S. Zhang, Z. Tan and J. Hou, *Macromolecules*, 2012, **45**, 9611–9617.
16 W. Zhao, S. Li, H. Yao, S. Zhang, Y. Zhang, B. Yang and J. Hou, *J. Am. Chem. Soc.*, 2017, **139**, 7148–7151.
17 Y. Ie, M. Nitani, H. Tada and Y. Aso, *Org. Electron.*, 2010, **11**, 1740–1745.
18 T.-Y. Chu, J. Lu, S. Beaupr, Y. Zhang, J.-R. Pouliot, S. Wakim, J. Zhou, M. Leclerc, Z. Li, J. Ding and Y. Tao, *J. Am. Chem. Soc.*, 2011, **133**, 4250–4253.
19 J. H. Hou, H.-Y. Chen, S. Q. Zhang, G. Li and Y. Yang, *J. Am. Chem. Soc.*, 2008, **130**, 16144–16145.
20 M. Scharber, M. Koppe, J. Gao, F. Cordella, M. A. Loi, P. Denk, M. Morana, D. Waller, Z. Zhu, X. Shi and C. J. Brabec, *Adv. Mater.*, 2010, **22**, 367–370.
21 Y. Ie, J. Huang, Y. Uetani, M. Karakawa and Y. Aso, *Macromolecules*, 2012, **45**, 4564–4571.
22 J. Huang, Y. Ie, M. Karakawa, M. Saito, I. Osaka and Y. Aso, *Chem. Mater.*, 2014, **26**, 6971–6978.
23 Y. Ie and Y. Aso, *Polym. J.*, 2017, **49**, 13–32.
24 H. Zhou, L. Yang, A. C. Stuart, S. C. Price, S. Liu and W. You, *Angew. Chem., Int. Ed.*, 2011, **50**, 2995–2998.

Open Access Article. Published on 22 August 2017. Downloaded on 7/28/2025 9:54:58 AM.
This article is licensed under a Creative Commons Attribution 3.0 Unported Licence.

25 B. C. Schroeder, Z. Huang, R. S. Ashraf, J. Smith, P. D'Angelo, S. E. Watkins, T. D. Anthopoulos, J. R. Durrant and I. McCulloch, *Adv. Funct. Mater.*, 2012, **22**, 1663–1670.
26 H. Bronstein, J. M. Frost, A. Hadipour, Y. Kim, C. B. Nielsen, R. S. Ashraf, B. P. Rand, S. Watkins and I. McCulloch, *Chem. Mater.*, 2013, **25**, 277–285.
27 M. Zhang, X. Guo, S. Zhang and J. Hou, *Adv. Mater.*, 2014, **26**, 1118–1123.
28 H. Zhou, L. Yang, S. Stoneking and W. You, *ACS Appl. Mater. Interfaces*, 2010, **2**, 1377–1383.
29 B. Yang, S. Zhang, Y. Chen, Y. Cui, D. Liu, H. Yao, J. Zhang, Z. Wei and J. Hou, *Macromolecules*, 2017, **50**, 1453–1462.
30 Z. Xiao, Y. Yuan, B. Yang, J. VanDerslice, J. Chen, O. Dyck, G. Duscher and J. Huang, *Adv. Mater.*, 2014, **26**, 3068–3075.
31 L. Zhao, S. Zhao, Z. Xu, Q. Yang, D. Huang and X. Xua, *Nanoscale*, 2015, **7**, 5537–5544.
32 Y. Ie, T. Sakurai, S. Jinnai, M. Karakawa, K. Okuda, S. Mori and Y. Aso, *Chem. Commun.*, 2013, **49**, 8386–8388.
33 S. Jinnai, Y. Ie, M. Karakawa, T. Aernouts, Y. Nakajima, S. Mori and Y. Aso, *Chem. Mater.*, 2016, **28**, 1705–1713.
34 S. Jinnai, Y. Ie, Y. Kashimoto, H. Yoshida, M. Karakawa and Y. Aso, *J. Mater. Chem. A*, 2017, **5**, 3932–3938.
35 S. R. Cowan, A. Roy and A. J. Heeger, *Phys. Rev. B: Condens. Matter Mater. Phys.*, 2010, **82**, 245207.
36 P. Schilinsky, C. Waldauf and C. J. Brabec, *Appl. Phys. Lett.*, 2002, **81**, 3885–3887.
37 V. D. Mihailetchi, H. X. Xie, B. de Boer, L. J. A. Koster and P. W. M. Blom, *Adv. Funct. Mater.*, 2006, **16**, 699–708.
38 L. J. A. Koster, V. D. Mihailetchi, R. Ramaker and P. W. M. Blom, *Appl. Phys. Lett.*, 2005, **86**, 123509.
39 M. M. Mandoc, W. Veurman, L. J. A. Koster, B. de Boer and P. W. M. Blom, *Adv. Funct. Mater.*, 2007, **17**, 2167–2173.
40 G.-J. A. H. Wetzelaer, N. J. Van der Kaap, L. J. A. Jan Anton Koster and P. W. M. Blom, *Adv. Energy Mater.*, 2013, **3**, 1130–1134.
41 L. J. A. Koster, E. C. P. Smits, V. D. Mihailetchi and P. W. M. Blom, *Phys. Rev. B: Condens. Matter Mater. Phys.*, 2005, **72**, 085205.
42 V. D. Mihailetchi, L. J. A. Koster, J. C. Hummelen and P. W. M. Blom, *Phys. Rev. Lett.*, 2004, **93**, 216601.

This journal is © The Royal Society of Chemistry 2017